Trans Indian Inst Met (2024) 77(8):1923–1937
https://doi.org/10.1007/s12666-024-03303-1

REVIEW

A Systematic Review on Microhardness, Tensile, Wear, and Microstructural Properties of Aluminum Matrix Composite Joints Obtained by Friction Stir Welding: Past, Present and Its Future

Rahul Biradar[1] · **Sachinkumar Patil**[1]

Received: 4 July 2022 / Accepted: 11 March 2024 / Published online: 4 April 2024

Abstract Friction stir welding (FSW) is a remarkable green solid-state joining process and it has been proven to be capable of joining advanced materials, such as aluminum matrix composites (AMCs) with sound-quality of joints. As a result, FSW is widely used in many sectors such as aviation, automotive, marine, and structural applications. So far various researchers carried out studies on joint characteristics of FSW and reported better microstructural and mechanical properties. This review study emphasizes various joint characteristics of AMCs namely microhardness, tensile, wear, and microstructural properties of joints obtained by FSW. Also, research work carried out by several researchers in the field of FSW for joining AMCs is summarized. In addition, future trends and challenges in joining of AMCs using FSW is presented.

Keywords Friction stir welding · Aluminum matrix composites · Hardness · Tensile · Wear and microstructure

1 Introduction

Advanced materials, such as aluminum matrix composites (AMCs), essentially replaced unreinforced aluminum alloys in recent years. It is because of their good mechanical and physical properties. AMCs are used in many applications, such as aircraft, automobiles, marine, and structural [1–3]. AMCs are a hot topic in today's material world because they possess high specific strength, low density, a high percentage of elongation, excellent fatigue resistance, creep, and wear resistance [4]. So far various reinforcements are utilized to fabricate different AMCs such as silicon carbide, silicon dioxide, titanium dioxide, aluminum nitride, titanium carbide, boron carbide, etc. But still, broad usage of these materials is restricted, due to a lack of advances in the development of joining processes and high production costs. Due to the low weldability of AMCs using conventional welding methods such as tungsten inert gas (TIG) and metal inert gas (MIG), therefore, it is necessary to employ novel friction stir welding (FSW) technique to join these materials to obtain sound joints [5, 6]. FSW could replace the traditional welding processes where joints are prone to the formation of various weld defects, such as porosity, cracks, distortion, etc. [7–9]. As a result, FSW is employed in various industrial sectors presented in Fig. 1. Previous works were reported that FSW can produce improved joint efficiency without porosity and solidification crack [10–12]. Particularly difficult to weld aluminum alloy series such as 2000, 6000 and 7000 series can be welded efficiently using FSW [13, 14]. In addition, FSW is capable to obtain better joints for dissimilar materials also. FSW process has certain benefits, some of which are: lower distortion, greater stability of weld structures, defect-free joints, and improved mechanical properties [15, 16]. Tool plays a crucial role in FSW, so far a variety of tool pin profiles were developed including cylindrical, conical, square, threaded, triangular, etc. and reported a significant impact of tool pin profiles on joint characteristics. FSW microstructural features consist of four different zones, such as stirred zone (SZ) or nugget zone (NZ), thermo-mechanically affected zone (TMAZ), heat-affected zone (HAZ), and base metal (BM) [17–19]. FSW joints yield better mechanical properties attributed to the formation of fine-grain microstructure.

✉ Sachinkumar Patil
sachindongapur@gmail.com

[1] School of Mechanical Engineering, REVA University, Bangalore, Karnataka, India

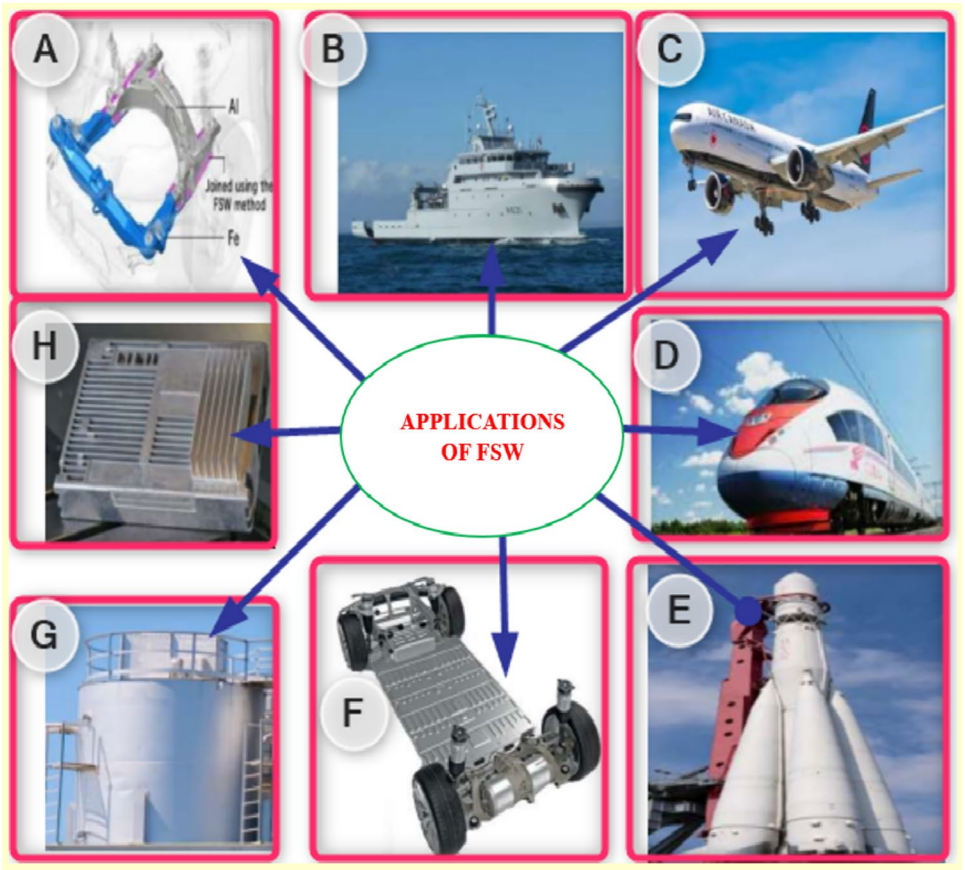

Fig. 1 Examples of the industrial applications of FSW: **a** Engine welded steel- Al engine cradle (Honda Accord model), **b** deckhouse structure of Littoral combat ship, **c** Eclipse 500 business jet, **d** floor panel of Shinkansen train, **e** Space launch vehicle panel, **f** electric vehicle battery tray, **g** liquid oxygen tank assembled by FSW, **h** electronic box (cooling fins)

This review study gives an overview of the FSW and the weldability of aluminum alloys and AMCs. Previous research works stated that FSW is a novel welding process for joining advanced materials. However, several challenges need to be overcome in FSW for joining of AMCs. This study focused on the hardness, tensile, wear, and microstructure properties of FSW joints. This review is of value to both researchers and scientists interested in understanding the evolution of microstructure during FSW and its correlation to the mechanical properties of joints.

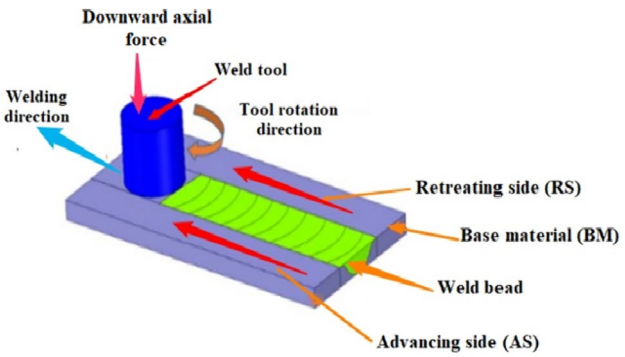

Fig. 2 Schematic representation of FSW process [17]

2 Brief Review of FSW

The Welding Institute (TWI) of the UK invented the FSW technique in the year 1991, as a solid-state joining method for obtaining aluminum alloy joints. In FSW, a rotating tool exerts pressure on the base metals, due to friction between the tool and the workpiece, heat is generated and a joint is obtained in a solid state as shown in Fig. 2. During the FSW process the material temperature reaches up to 80% of the melting temperature and this method can be classified as one of the hot working process [20]. FSW is particularly useful for joining high-strength non-weldable alloys that are highly susceptible to solidification cracking and liquidation cracking. FSW is preferred because of its minimum energy consumption, no harmful gas emissions, and no need for consumable materials, filler materials, and shielding gases [21]. FSW is generally considered a sustainable welding technology and its usage has accelerated, replacing 10% of the joining process. In general, FSW joints produces defect free welds, fine microstructure, and no distortion resulting in better strength of the joints [22]. However, it is observed that weld strength varies along the

joint. Particularly, at the starting and end point of the joint, lower weld strength has been observed as shown in Fig. 3.

3 FSW Process Parameters

FSW process parameters play a vital role in obtaining sound joints. However, FSW parametric window is narrow for joining AMCs compared to unreinforced alloys. The strength of weld joints depends mainly on the proper selection of parameters, such as tool rotation speed, welding speed, axial force, tool pin profile, tool tilt angle.

Compared to the above-mentioned FSW process parameters, tilt angle contributes less to decide the strength of joints. However, tilt angle alters the flow of material and controls weld defects [23]. Usually three tilt angles (0°, 1° and 2°) were used by several researchers [24–27]. Tilt angle helps to apply downward forging force needs to be increased with increasing tilt angles, and this results in more frictional heat generation as shown schematically in Fig. 4.

Usually, joint strength decreases as the process parameter values exceed the optimum values due to the formation of defects at higher speed or lower speed [28]. Proper selection of these process parameters yields sound joints without any defects like tunnel defects, pinholes, and cracks [29, 30]. Use of traditional experimental methodologies to identify the effect of process parameters, such as maintaining one parameter constant while changing the other parameter, result in increased time consumption and less accuracy. There are various techniques for achieving the required output by framing novel models to overcome this problem. Among the various statistical tools available to optimize the FSW parameters, the Taguchi tool is considered one of the simple techniques. The Taguchi tool is typically used to optimize process parameters to improve product quality [31]. In addition, sound quality welds could be obtained for dissimilar joints as well using the Taguchi approach, as a result improvement in the tensile properties of the dissimilar joint is observed [32]. Analysis of variance (ANOVA) studies

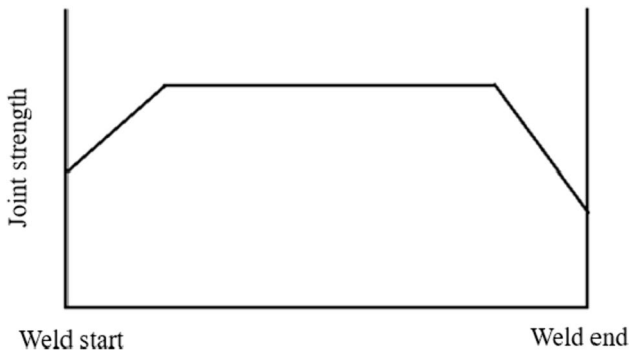

Fig. 3 Schematic of strength variation along a butt joint [19]

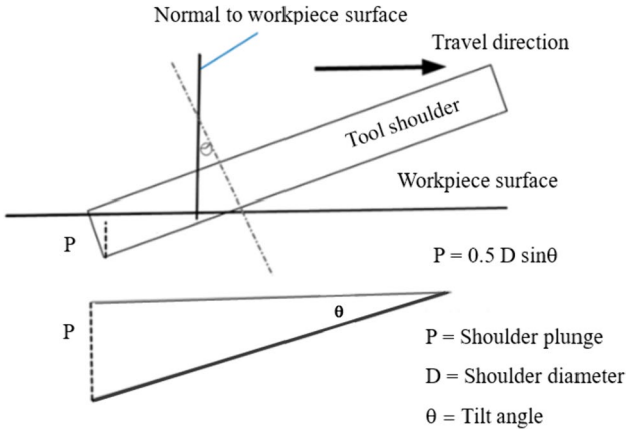

Fig. 4 Cross-sectional view of a tool tilt during FSW [19]

reported that tool rotational speed and traverse speed are the most dominant process parameters to decide the strength of the weld joints. Further, several studies have been reported on mathematical modelling of FSW joints and are evaluated using response surface methodology (RSM). RSM can be used effectively to develop a correlation model and predict the quality of FSW joints [33, 34].

4 FSW Tool

The tool is the heart of the FSW process. Figure 5 shows schematic of FSW tool; FSW tool pin profile significantly contributes to heat generation and affects the quality of

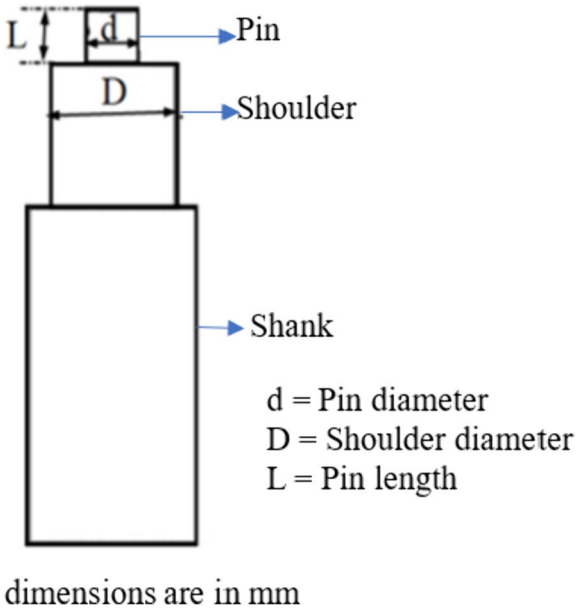

Fig. 5 Schematic of FSW tool parameter [17]

welds. Tool helps to soften the material due to friction and leads to the flow of plasticized material, resulting in the formation of a joint in the solid state. The FSW tool consists of two parts, namely, pin and shoulder. The design of the tool plays crucial role to the success of the FSW process. FSW joint strength directly depends on mixing of plasticized material during the process.

Researchers developed several tool pins profiles to get better joint properties, such as cylindrical, square, tapered, and threaded, as shown in Fig. 6. In FSW, the tool decides the mode of plasticized material flow, weld size, and weld speed. Tool stimulates plastic flow during the process and can produce a refined grain size resulting in better strength of the weld joint [35, 36]. Previous works reported heterogeneous microstructure and mechanical properties for different tool pin profiles. Singh et al. [37] used several tools, namely conical, pedal, threaded cylindrical, triangular, square and pentagonal. It was observed that, weld strength was significantly improved for the joints obtained using square tool and resulted in better joint efficiency of 78% obtained for AA2024 joints. In addition, EBSD analysis witnessed presence of recrystallized finer grains in nugget zone as a result of dynamic recrystallization. Further, Hasan et al. [38] obtained better joints, for 10 mm thick plates of A356 alloy. Joints were obtained using several reinforcements such as ZrO_2, SiC, B_4C, and TiC by employing different tool pin profiles namely square, cylindrical, and threaded tool. Reinforcement particles were not dispersed uniformly by cylindrical and threaded tool. However, particle distribution is almost homogeneous by square tool due to higher eccentricity and there is no vertical motion of the material observed. The square pin produces highest temperature compared to other pin profile and results in better material flow. In addition, Yuvaraj et al. [39] used high-speed steel tool for FSW with pin profiles like square, cylindrical, and triangular shape. Better mixing of material was observed for cylindrical and triangular tools compared to square tool. Moreover, Janeczek et al. [40] performed FSW for joining AW 3004 (Al Mn Mg alloy) using cylindrical and taper threaded tool. It was noted that material flow for cylindrical threaded pin was better than that of taper threaded pin. Insufficient heat input leads to FSW defect in the form of void for taper threaded tool, where material is not stirred fully to obtain a joint results in lower weld strength. The use of cylindrical threaded pin results 37% higher strength compared to taper threaded pin. Interestingly, Nidhi et al. [41] mentioned that the material movement from front to back of tool depends on static volume to swept volume ratio (ST/SW). Square pin profile possess the maximum ST/SW ratio and it provides better pulsating action, therefore material undergo better stirring compared to cylindrical, taper, cylindrical cam, taper cam and square shape. Further, Sanjeev Verma and Vinod Kumar [42] reported better joint characteristics for cylindrical tool for joining aluminum alloys. It is due to higher amount of frictional heat generated, due to rubbing action between the tool and workpiece. Also, Ashu et al. [43] designed several tools of FSW for obtaining better quality joints. Tools namely, cylindrical grooved (CG), cylindrical grooved with flutes (CGF), cylindrical full threaded (CFT), cylindrical full threaded with flutes (CFTF), cylindrical half threaded (CHT), square (SQ) and cylindrical tapered (CT) were designed, and observed the fine grains and more homogeneous microstructure, highest strength for CGF and CG tools. It is due to stronger stirring action and dynamic recrystallization of the grains. Higher angle grain boundaries (HAGBs) are predominant when compared with grain boundaries distribution for other pin profiles. Fine equiaxed grain structure consists of the dislocation movements during tensile loading and it creates pilling at grain boundaries to allow the plastic flow and it exhibits the higher strength. Interestingly Zhou et al. [44] welded Al-Cu dissimilar sheet of thickness 2 mm by using circular pin, circular threaded and circular threaded with flutes. By using circular threaded pin, Cu easily diffused into the aluminum between the hook and keyhole to form hard and brittle intermetallic compounds. Not much difference was observed in the microhardness distribution. Maximum tensile shear failure load is reported for threaded tool pin. Table 1 represents different FSW tool pin profiles and their significant observations.

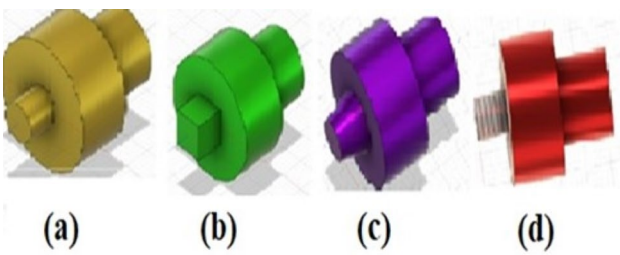

Fig. 6 Several commonly used FSW tool pin profiles **a** cylindrical tool, **b** square tool, **c** cylindrical tapered, **d** cylindrical threaded tool [7]

5 Weldability of Aluminum and Aluminum Matrix Composites

The strength of pure aluminum and its alloys is insufficient for various applications. Therefore, aluminum alloys are mixed with reinforcements, resulting in new materials called AMCs. Joining of AMCs using the fusion welding process exhibits issues like a decrease in strength and formation of defects [58]. AA1000, AA3000, and AA5000 series of weldable aluminum alloys are reinforced by working in cold, whereas the AA2000, AA6000, and AA7000 series precipitation hardening can be used to strengthen heat-treatable

Table 1 FSW tool pin profile with different shape of geometry and observed importance during FSW process

Sl. No	Authors	Tool pin profiles used	Significant observation
1	Singh et al. [37]	Square, triangle, conical pedal, pentagonal and threaded cylinder	Significant performance enhancement observed using square pin tool
2	Jancezek et al. [40]	Threaded pin with cylinder and taper	Better joint efficiency is obtained using tapered threaded tool
3	Nidhi Sharma et al. [41]	Square, taper cam, cylinder, and cylinder with cam profile	The material is properly mixed in nugget zone with square pin tool
4	Varma et al. [42]	Square, straight, and tapered cylinders	Good weld quality is reported for straight cylindrical tool
5	Ghiasvand et al. [45]	Dual pin tool	Dual pin led to microstructural evolution resulted in grain growth and better material flow
6	Shimpi et al. [46]	Cylindrical and triangular tool	During FSW temperature is greatly influenced by cylindrical pin
7	Kumar et al. [47]	Cylinder with threaded and straight cylindrical	Noted, higher joint efficiency for threaded cylinder tool
8	Kumar et al. [48]	Triangular, taper with thread and hybrid	Hybrid tool is given good performance
9	Battaiana et al. [49]	Hexagonal, cylinder, square, pentagon and taper square	Good grain size is obtained by square pin tool
10	Jayaprakash et al. [50]	Cylinder, taper and triangle	Higher tensile strength obtained for triangular pin
11	Bokov et al. [51]	Cylinder and frustum	Sufficient heat is generated by cylindrical pin
12	Pranish et al. [52]	Cylinder, square, hexagonal, tapered hexagonal,	Better performance obtained for tapered hexagonal joints
13	Sun et al. [53]	Conical threaded and conical cam thread	Better joint performance is reported for better performance
14	Rahul et al. [54]	Square and taper conical threaded	Powder particles homogeneously distributed during welding with taper conical threaded pin
15	Nikul et al. [55]	Cylindrical, threaded, and taper cylinder	Threaded cylinder pin yielded sufficient heat generation
16	Yang et al. [56]	conical threaded of different root diameter and pin diameter	The thickness of intermetallic compound and eutectic layer interface is positively corelated
17	Ramchandran et al. [57]	Straight cylinder and tapered cylinder	Higher intermetallic bond is formed by tapered cylinder tool

alloys [59–61]. FSW could achieve sound joints for various AMCs reinforced with SiC, Al_2O_3, B_4C, TiB_2, and ZrB_2. The literature stated that these AMCs can be joined successfully using FSW. Generally, the microstructural evolution in the FSW zone occurred due to dynamic recrystallization, as a result, fine-grain microstructure with high-angle grain boundaries was observed. In addition, each zone of FSW exhibits a different thermomechanical condition, precipitation, and dislocation behaviors resulting in different hardness in different zones [62].

FSW process involves several processes such as heating, cooling, and plastic deformation as well as the flow of material around the tool as shown in Fig. 7. During the process two workpieces are joined by supplying heat in the solid state. The amount of heat input causes microstructural changes, such as recrystallization, grain orientation growth, and dislocation of strengthening precipitates [63–65]. Also improper supply of heat results in the formation of defects such as nonbonding, void formation, flash defects, kissing bond, zigzag defects, tunnel defect,

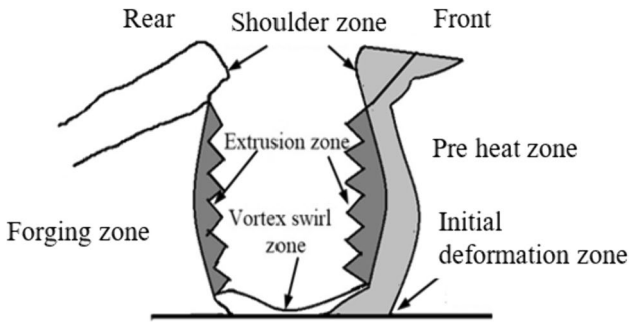

Fig. 7 Schematic of material flow pattern during FSW [63]

and an onion ring. Due to the improper flow of plasticized material (Fig. 8a), joints undergo the formation of tunnel defects and cavities as shown in Fig. 8b. Further, the onion ring occurs at very cold-welding conditions, due to insufficient material flow and can be observed as bands in the nugget zone as shown in Fig. 8c.

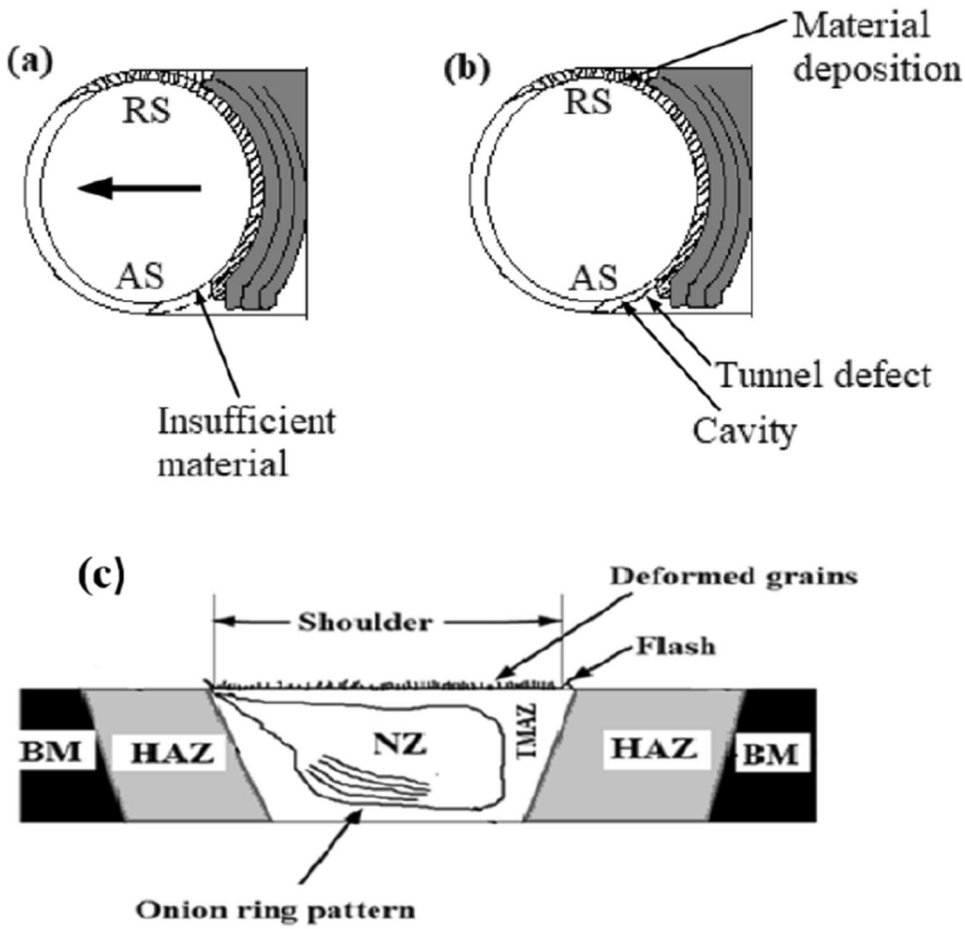

Fig. 8 Schematics of **a** material flow pattern, **b** formation of tunnel defect and cavity and **c** formation of onion ring in nugget zone [19, 22]

6 Dissimilar Friction Stir Welding (DFSW)

For several applications, it is necessary to obtain the joints between two dissimilar materials such as aluminum, copper, steel, and other material. Such joints can be obtained using dissimilar friction stir welding (DFSW), focused on friction heat produced by a simple tool to soften and stir materials together by rotating and traversing the tool. DFSW has several advantages, including a less cost and simple operation procedure resulting in the widespread use of the FSW process for dissimilar joints. DFSW joints exhibit better mechanical properties such as tensile strength, hardness, yield strength, and percentage of elongation compared to TIG/MIG weld joints. DFSW successfully minimizes the defects, however, a few minor defects occur, such as fragment defects, surface cavities, and flash formation [66] due to differences in the melting point of the materials. Here, discussed a few of the researcher's opinions on DFSW. AA7075 to AZ31 Mg alloy joints were obtained successfully and observed that the formed intermetallic influenced the weld quality. AA7075 alloy and AZ31 alloys are structural components with high specific strength but their weldability is poor, limiting their applications. So, DFSW can become a candidate for joining such different materials [67]. Similarly, AA5182/AA6061 dissimilar aluminum alloy joints can be obtained by FSW. Such combinations of materials are used in the automobile industry for joining the side wall and back wall because they combine toughness, weldability, and better strength. Mg and Si are the hardening precipitates used to strengthen 6061 aluminum alloys. Si can improve its fluidity and resistance to hot cracks, while Mg can boost its specific strength. High-magnesium content aluminum alloys such as AA5182 have outstanding formability and deeply extended forming as this material is broadly used in the manufacturing of automotive parts [68]. In addition, aluminum/titanium hybrid composites with good properties can be used in a variety of applications, including the automobile and aircraft industries to improve fuel efficiency. Due to the differences in physical and mechanical properties such as thermal conductivity, density, strength, and hardness, it is difficult to join Al and Ti alloys using traditional welding procedures, which restricts the use of Al/Ti structures in various applications [69]. Similarly, electrical components, transformer foil conductors, condensers, capacitor foil windings, heat transfer tubing, freezer tubes, and tube covers are all common uses for aluminum and copper dissimilar joints [70]. Aluminum

or magnesium alloys are most often used in the lap and butt configurations to join dissimilar materials. Using DFSW, efficient joints could be produced with sound qualities compared to conventional welding methods [71].

7 Mechanical Characteristics of FSW Joints

7.1 Microhardness Characteristics

In this section, the microhardness of FSW and its trends are discussed. It is noted that different microhardness profiles have been observed for various AMCs. Some of the researcher's opinions on the microhardness of FSW are discussed here. The addition of nano-level reinforcement powder such as Al_2O_3 and SiC increased the microhardness of weldments [72]. General trends of FSW hardness profile in different zones are shown in Fig. 9. The hardness drops substantially from the NZ to the BM. The advancing side exhibits a higher hardness value than the retreating side; therefore most of the weld joints have undergone fracture in the retreating side [73]. Bozkurt et al. [74] performed interlayer hardness measurements, and a minor difference in hardness was found between the base composite and weld nugget. The microhardness values for the base composite were around 185 HV. Hardness decreased up to 170 HV on the root side and 165 HV on the top. It is understood that rapid heating and cooling will result in variations in temperature between the reinforcement and matrix interface. The HAZ region covers less heat than the weld nugget. As a result, the driving force provided to produce discontinuities in the HAZ resulted in a reduced hardness of 155 HV compared to the base metal.

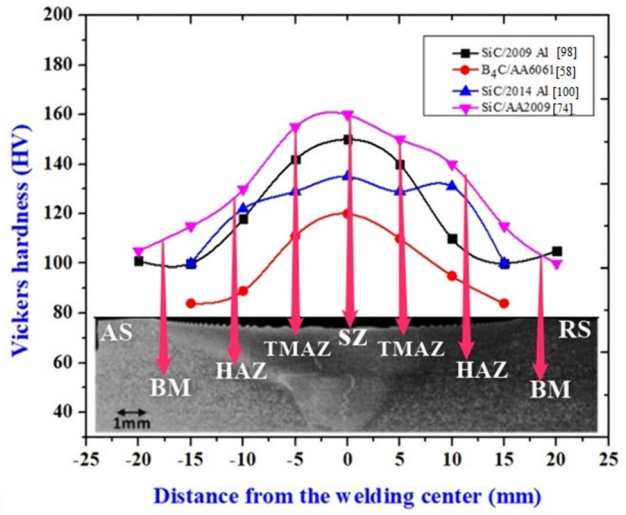

Fig. 9 Hardness profile in different zones of FSW on advancing and retreating side [71, 83–85]

Microhardness distribution is depending majorly on tool rotational speed, for example for Al-Li alloy hardness varied from 128 to 158 HV for 595–1000 rpm tool rotational speed [75]. The microstructure is significantly influenced by the rotation speed, which impacts the microhardness of the joint. In most cases, FSW joints exhibit a typical "W" shaped hardness profile from the weld center. The microhardness of weld joints is also depending on several parameters such as particle density, heat treatment, and grain size. In an investigation [76] two distinct joints with the highest and lowest heat inputs were produced to check the impact of heat on hardness. The NZ has a higher hardness than the base metal. The increase in microhardness in the NZ is due to either primary tempering or room temperature condition of the base material. In a study on FSW of AlSi10Mg and its composites, hardness was greater than that of the conventional AA6061-T6 alloy. It is due to the homogeneous distribution of grains and hardening of Mg_2Si precipitates. Weldment exhibits a reduction of hardness. Weld strength decreased from 107 HV at the base metal to 66 HV at the NZ. Reduction in hardness is attributed to metallurgical transactions that took place during welding [77]. Also, the dissolution of the strengthening precipitates causes the NZ to soften, therefore the NZ hardness value decreases. Due to the presence of a low strengthening effect phase and coarse grain structure in HAZ, the hardness value is lower than the NZ [78]. The advancing side hardness value is lower than the retreating side. This is due to more heat generation on the advancing side than on the retreating side. As a result, there is more material deformation and softening on the advancing side so the hardness value on the advancing side is lower than on the retreating side. Also, FSW increased the hardness of composites. TMAZ and HAZ exhibited varying hardness. In TMAZ, B_4C particles have a band-like structure that helps to improve toughness. In NZ, dynamic recrystallization produces finer grains and particles [79, 80]. The general trend in FSW hardness of AMCs is, that after FSW the hardness value increases due to the stirring action of the tool, causing abrasion of reinforcement particles minimizing their size and uniform distribution. HAZ exhibits a hardness value lower than the base material. Because of the heating effect, grain softening occurs, resulting in a decrease in hardness [81]. Generally, hardness distribution throughout the weld region shows symmetric profiles on either side of the weld center. In addition, dissimilar FSW of Al-Cu joints also reported better microhardness on either side of welds [82]. However, the hardness gradually decreases from the base material to the NZ due to variation in thermodynamic cycles in various zones.

7.2 Tensile Characteristics

Tensile characteristics of FSWed joints play a major role in understanding the stress versus strain behaviour of weld joints, which also depicts the strength and fracture properties of weld joints. In this section FSWed yield strength (YS), ultimate tensile strength (UTS), and percentage elongation are discussed. Unsurprisingly, variation of strength is reported in most of the cases. FSW process parameters especially, tool rotational speed and welding speed have a major impact on strength. For example, FSW of aluminum and bronze joint, at 20 mm/min, UTS of 94.5 MPa, and elongation of 15.5% is observed and the UTS and elongation were 89.4 MPa, and 13.8%, respectively, at a welding speed of 25 mm/min [86]. It is noted that the impact of water cooling and air cooling on FSW joints is also remarkable. The UTS of the water-cooled joint is maximum than the air-cooled joint for AA7075 [87]. Further, a study [88] reported a reduction of strength after FSW as depicted in the stress versus strain diagram shown in Fig. 10. Accordingly

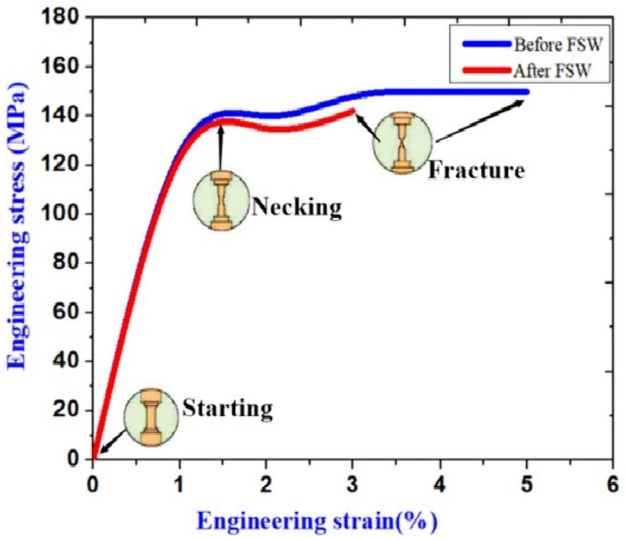

Fig. 10 Stress versus strain curve for AA6061/SiC/flyash base composite and FSWed joint [88]

reported a UTS of 164 MPa and a % elongation of 9% before FSW. Also, UTS of 139.5 MPa, and a % elongation of 5% after FSW. AMCs joint strength is influenced by the initial and final conditions of parent metals and joints; as a result variation in the strength of the joint is observed. The load-carrying capacity of the AMCs has increased as a result of the lack of gaps or pores encircling the reinforcing particles [89]. As a result, 85% joint efficiency is obtained [83]. Also, better strength is reported in dissimilar joints between AA7075 and AZ31. When the speed is increased from 200 to 1200 rpm, UTS varies from 55 and 250 MPa [90]. Further, Bozkurt et al. [74] reported an FSW of 25%SiCp/AA2124 and presented results as tabulated in Table 2. The efficiency of the joint was nearly 80%. The high joint efficiency is due to grain refining within the stir zone. Several studies reported a decrease in strength after welding due to differences in reinforcement particle size, shape, and distribution in the weld zone [91]. Also, sometimes joint undergoes fracture at the center of the weld nugget, due to lesser strength than the base metal, and continuous yielding was observed [92]. The smooth interface between the SiC particles and the aluminum matrix is increasing UTS. Further, in most of the cases, the tensile specimens have undergone fracture in the HAZ, due to less hardness [93]. Figure 11a and b shows UTS trends for various spindle speeds and welding speeds. These figures imply that better strength of weld joint is obtained for optimal spindle speed and welding speed showing trends similar to the bell curve. However, UTS of the weld is seen to increase between 405 and 445 MPa and then decrease to 427 MPa. At 800 rpm speed, the maximum value of UTS is obtained with a joint efficiency of 83% for AA2060 material [94]. Further, Hu et al. [95] noticed that the weld joint in comparison had almost same tensile strength as that of base metal. With a travel speed of 300 mm/min, the percentage elongation and UTS were 12.5% and 206 MPa, respectively. With a welding speed of 100 mm/min, the elongation was 12.3% and UTS was 203 MPa. In some cases, an increase in tool rotation speed improves the UTS and the joint strength gradually increases with varying welding speeds due to the material flow. In addition, several researchers have reported on the joining of different AMCs using FSW and obtained

Table 2 Tensile tests results of the base composite and the FSWed joint

Material	Rotation speed (rpm)	Transverse speed (mm/min)	UTS (MPa)	Elongation (%)	Joining efficiency (%)
25%SiCp/AA2124 [74]	NA	NA	450–461	2.3–2.5	NA
FSWed 25%SiCp/AA2124 [74]	1120	40	408	1.4	90
			346	1.2	76
			344	1.6	76
			±366	±1.4	±81

NA: Not applicable

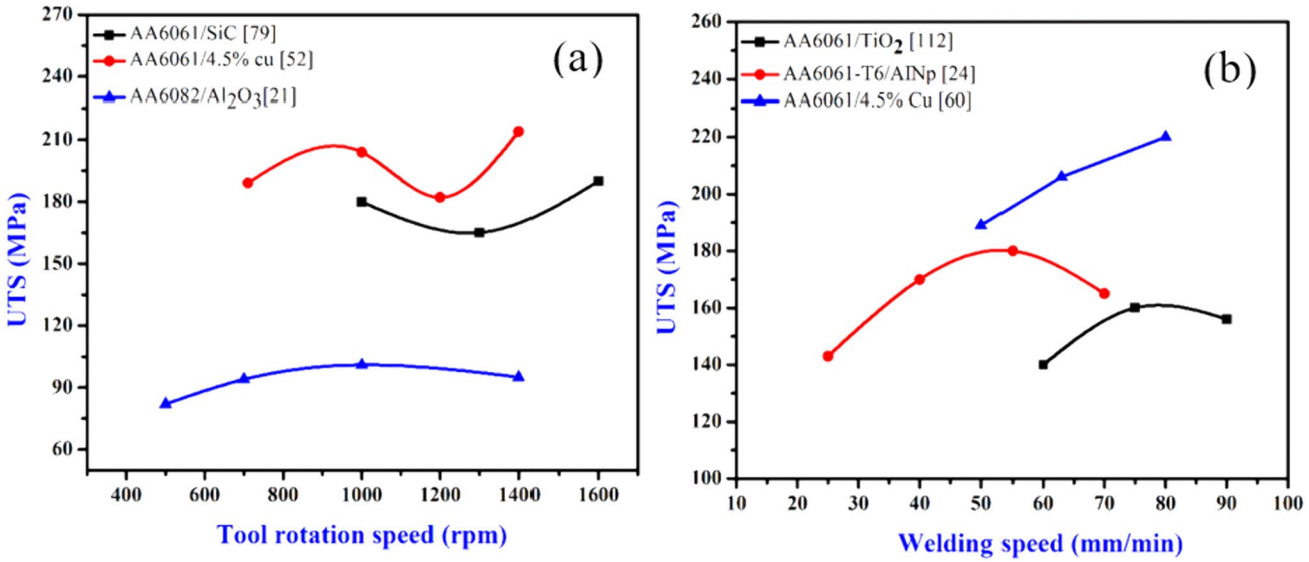

Fig. 11 Effect of **a** tool rotational speed on UTS [21, 65, 94] and **b** welding speed on UTS [24, 73, 100]

the maximum joint efficiency of 108% for AA2009-T4/SiC/15% and the highest UTS of 581 MPa for AA2009-T4/SiC/17%. Similarly, the maximum hardness is 160 HV for AA2009-T4/SiC/18% is reported as presented in Table 3. Unsurprisingly, tool pin profile also has a significant effect on UTS and Hardness. Various tool pin profiles have an impact on joint strengths. Literature evidenced that the square tool yielded higher strength and the triangular tool yielded less strength for FSW joints [38, 96–99].

7.3 Wear of FSW Tool

FSW tool wear can be influenced by process parameters like rotating speed (r), welding speed (v), joint length (L), and tilt angle. It was noted that tool wear is caused by material flow rather than material drag and it is proportional to v and L. Also suggested that abrasive wear occurs where the reinforcements radius exceeds the shear zone's width at certain locations, % of wear in FSW is given by Eq. (1).

Table 3 Mechanical properties of various FSWed AMCs

Sl. No	AMCs	D/d (mm)	SR/TS (rpm/mm min^{1})	HV	YS (MPa)	UTS (MPa)	Elongation (%)	Joint efficiency (%)
1	20%AIN/AA6061-T6 [29]	18/6	1200/55	–	–	241	–	93
2	AA6063/B_4C/12% [79]	–	1000/78	105	–	201	2.5	93.4
3	20%Al_2O_3/AA6061-T6 [101]	–	450/150	–	234	251	–	70.7
4	AA2009-T4/SiC/15% [84]	24/8	600/50	155	250	325	2	18.33
5	10%Al_2O_3/AA6061-T6 [102]	–	800/56	104	280	329	1.3	–
6	20%Al_2O_3/AA6061-T6 [103]	–	800/56	50	193	262	2.8	71.98
7	22%Al_2O_3/AA6061-T6 [104]	15/4	630/115	90	–	227	–	99
8	10%/SiC/AA6061 [105]	18/6	1100/45	–	200	278	8.0	74
9	AA6061/SiC/20 [106]	–	1370/89	114	201	265	–	–
10	Al4.5%Cu/TiC/10 [100]	–	40/20	–	–	178.9	2.95	–
11	AA6061/ZrB_2/10 [107]	–	1155/49	–	–	242.56	–	90
12	AA2009-T4/SiC/15% [108]	20/8	800/100	–	344	521	7.1	–
13	AA2009-T4/SiC/17% [91]	–	1000/800	160	341	501	3.5	97

PT: Plate thickness; D/d: shoulder diameter/pin diameter; SR/TS: speed of rotation/transverse speed

$$\%\text{Wear} = \frac{5.D.\Delta C\max.f\text{v}.\omega.L}{24.R.v} \quad (1)$$

where D is diameter, f_v is the volume of fraction, R is the radius, and the C_{max} is the cutting arc's maximum value. Tool wear is more noticeable in FSW of hard particle reinforced AMCs.

Soft metals such as aluminum and magnesium, cause no serious wear rate. When welding hard metals and AMCs, wear rate becomes more. For many of the materials, the tool wears during FSW and reported that the wear rate is inversely proportional to the material's hardness [109]. Although, better wear performance has been achieved for a particular combination of process parameters so that hardness increased and wear rate reduced. Also, tool initial wear can be deferred by lowering tool rotation and increasing the welding speed over time [89]. Further, harder materials other than steel could be used as tool materials to reduce the wear rate [110]. In addition, the wear rate of several tool materials including steel, WC–Co micro, WC–Co submicron, and WC–Co coated with diamond, was recently compared by researchers, and tool wear is reduced by 60–80% by using coated tools. Compared to the uncoated sample, the AlCrN coated sample had better wear resistance and lost about 87% less weight [111, 112]. Several researchers stated that wear is the function of spindle speed and welding speed. In a study [113] wear rate was evaluated at various transverse speeds and observed that a welding speed of 45 mm/min was combined with a rotation speed of 1250 rpm to achieve the maximum wear rate. A wear rate increased by 6% as the welding speed increased from 35 to 45 mm/min. The wear rate dropped significantly when the welding speed increased from 45 to 65 mm/min. Also, the wear rate of the FSW joint of Ni-coated AA6061 plates drastically decreased at 1000 rpm and 28 mm/min, as well as 1400 rpm and 56 mm/min, when compared to the sheets without coating. As a result, a higher tool rotation speed (i.e., 1400 rpm) should be preferred for better wear properties of Ni-coated AA6061 joints [114]. However, severe tool wear occurred for Al_2O_3p/6061Al composite. The wear rate of the tool increases linearly with an increase in linear welding distance [115]. Generally, an increase in the sliding distance led to increased values of wear rate and weight loss [116]. In some works, it is mentioned that the abrasive wear mechanism is dominant in FSW tool wear. Shojaeefard et al. [117] studied composites reinforced by TiC and B_4C, the abrasive wear component was found to be the dominant wear mechanism. Moreover, the wear specimen area of the TiC composite is smoother than that of the B_4C composite, indicating that the TiC composite has higher wear resistance. Interestingly, FSW tool geometry also influences tool wear, as noted by Shindo et al. [118] for SiC/Al359 composites using threaded pin tools with no holes that produce homogeneous welds without imposing excessive tool wear. Moreover, lesser tool wear for tools having fewer threads on them [101]. In a comparative study [119], a comparison of the wear of O1 steel tools and WC/Co tools was performed. Even though the WC/Co tools had a higher wearing resistance than the O1 steel tools, the WC/Co tools were worn out, with a volume loss of about 4.23% during welding for 1320 mm. When the welding speed was reduced, the tool's wear rate increased. During the initial welding operation, the maximum wear rate is obtained [84]. For example, while welding 240 mm, the pin diameter was reduced by 11%. At the maximum-wear area, the pin diameter was reduced by 27% after welding 1800 mm. Sometimes it is noticed that the formation of TiC and TiB_2 hard phases during dry sliding wear test conditions at 20 °C, 300 °C, and 600 °C for HBN-coated tools [120].

In summary, considerable tool wear occurred when steel tools were utilized to weld the ceramic particles reinforced AMCs. Moreover, the mechanical properties of the joints would be affected as a result of the particle wear. The coated carbide tool could perform well for composites with a particle volume fraction of less than 30% without causing excessive wear.

8 Microstructural Characteristics

The mechanical properties of joints depend on the microstructure of weldment. The microstructure of the FSWed joint depends on various variables, such as weld parameters, tool material, tool type. In this section, the microstructural characterization of FSW joints is discussed. As mentioned in previous sections, FSW consists of four zones such as NZ, TMAZ, HAZ, and BM. In FSW, material flows in a complex pattern on the advancing side and retreating side. As a result, different grain structures with grain sizes are observed in various zones as can be seen in Fig. 12.

Insufficient plastic deformation in TMAZ has been observed due to a lack of heat supply resulting in different microstructures than NZ. The FSW tool stirring action results in the formation of fine grains in the NZ. The advancing side of the joint is defined by a strong separation compared with TMAZ and the NZ. But, the microstructure of the retreating side of the weld joint is more complicated and the edge between TMAZ and NZ is unclear in most cases. This is because of differences in tool rotation and welding direction between the advancing side and the retreating side. As a result, temperature transfer in the flow of material and mechanical properties on both sides of the welds are asymmetrical. Whenever a sufficient amount of heat is supplied to the base metal, defects such as wormholes and piping defects are absent, as the heat is sufficient to exceed the reinforced material's flow stresses to produce sound weld joints [85].

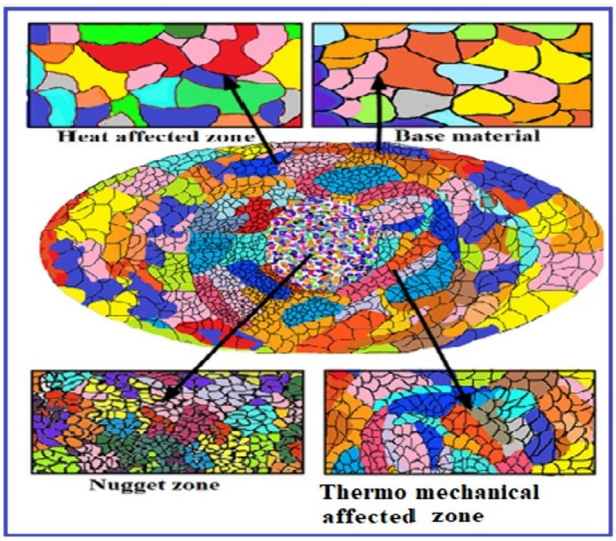

Fig. 12 Inverse pole figure (IPF) orientation map with grain boundaries on different zones of FSW [17]

A study [121] reported a decrease in grain size from the upper nugget zone (UNZ) to the lower nugget zone (LNZ). UNZ was subjected to a great amount of centrifugal force and more heat was supplied at top of NZ compared to UNZ and LNZ. As a result, the hardness of UNZ is lower than that of LNZ. Because of differences in deformation and high-temperature differences at various sections of the weld joint and grain size decreases from 7 to 3 µm as shown in Fig. 13. Furthermore, the reinforcement phase distribution in the matrix appears to be fairly uniform. The stir zone which is typical of FSW is evidenced by significant grain deformation and dynamic recrystallization. After being stirred by the probe, the large reinforcement particles in this region are separated into equiaxed. The reinforcement particle dispersion in the matrix was found to be closely uniform with estimated average particle sizes of about 0.6–0.1 mm in the NZ [122]. Next to the NZ is TMAZ which has elongated grains that are inclined in one direction. In TMAZ, the combined effects of heat and plastic deformation result in insufficient strains to cause recrystallization. However, HAZ only experiences heat changes and no plastic deformation. Grain growth occurs

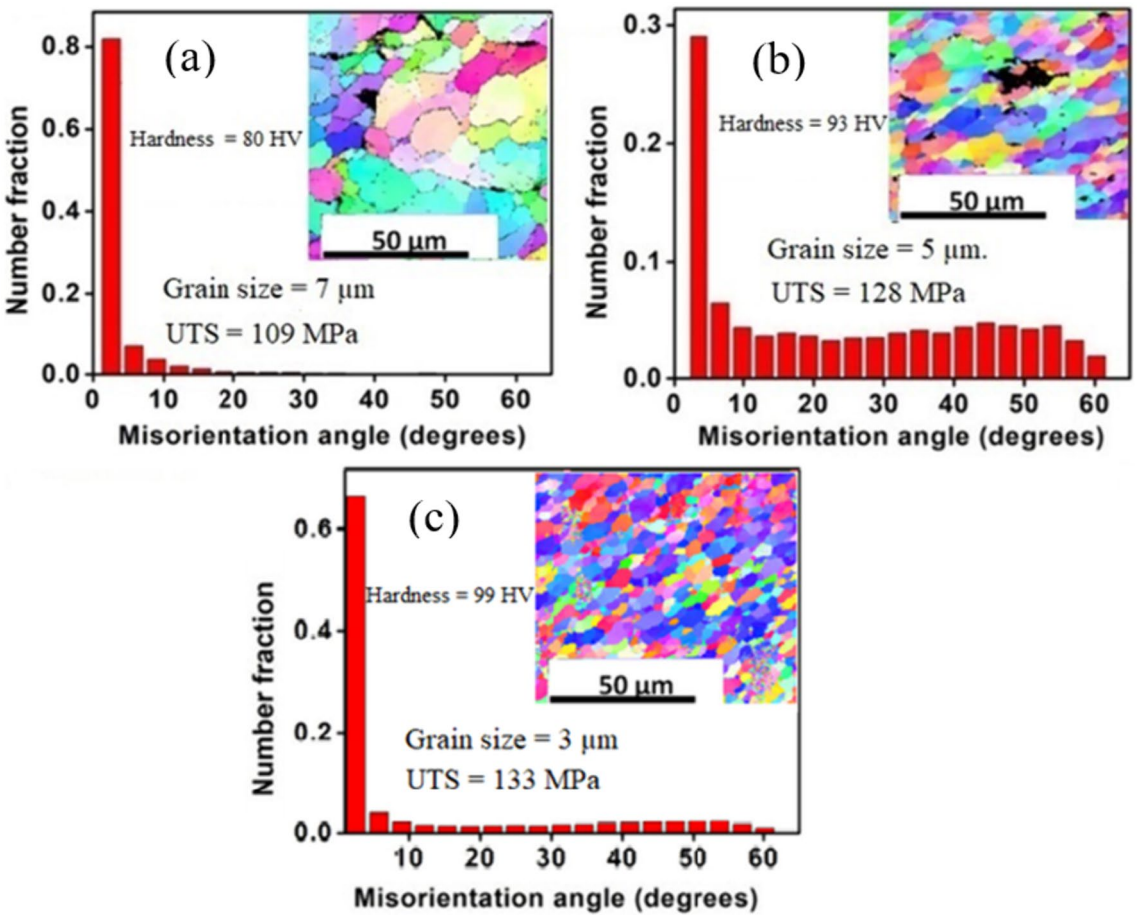

Fig. 13 EBSD images showing the grain orientation at (a) UNZ (b) MNZ and (c) LNZ [121]

in this region as a result of the heating. Finally, there is no change in grain size in the base material region because there is no effect of plastic deformation or heat [81]. The TMAZ grains on the advancing side were found to be slanted upward for the tool direction. As the weight percent of reinforcement increased, the grain size decreased. At 6 wt% reinforcement, the grains were larger and at 9 and 12 wt%, the grains were smaller. The reinforced particles in the aluminum matrix were also found to be evenly distributed [78]. The grain size is mainly depending on the amount of heat supply. Grain size is finer when the amount of heat input is sufficient and also high-angle grain boundaries (HAGBs) were observed [123]. Guo et al. [124] reported the formation of fine equiaxed grains and partially elongated grains in TMAZ with a grain size of 9 µm in the base material and 4 µm in the NZ. In addition, Sachinkumar et al. [88] reported the formation of HABs with an average grain size of 3.4 µm attributed to the evolution of microstructure during FSW as shown in Fig. 14. Also, HAZ is subjected to frictional heating, resulting in coarser-grains-than-the-base metal. The TMAZ has more deformed and finer grains than HAZ and base metal [125]. Because of the probe stirring and frictional heating, a portion of the precipitates is extended along with the material flow. The NZ has a more compact structure around the keyhole than the TMAZ which is characterized by sophisticated and equiaxed grains [126]. Further, the tool pin profile also having a significant impact on grain size. The grain size of FSW joints was obtained using different tool pin profiles as shown in Fig. 14a–d. Compared to different tools, a higher grain size (8.5 µm) was observed for the cylindrical tool, whereas fine grains with a grain size of 3.4 µm were observed for joints obtained by the square tool compared to other tools. Figure 14b shows the fine grains produced by the square tool pin, which is due to a greater number of flat faces on the tool, which is leading to sufficient heat generation, resulting in a higher degree of deformation than other tool profiles.

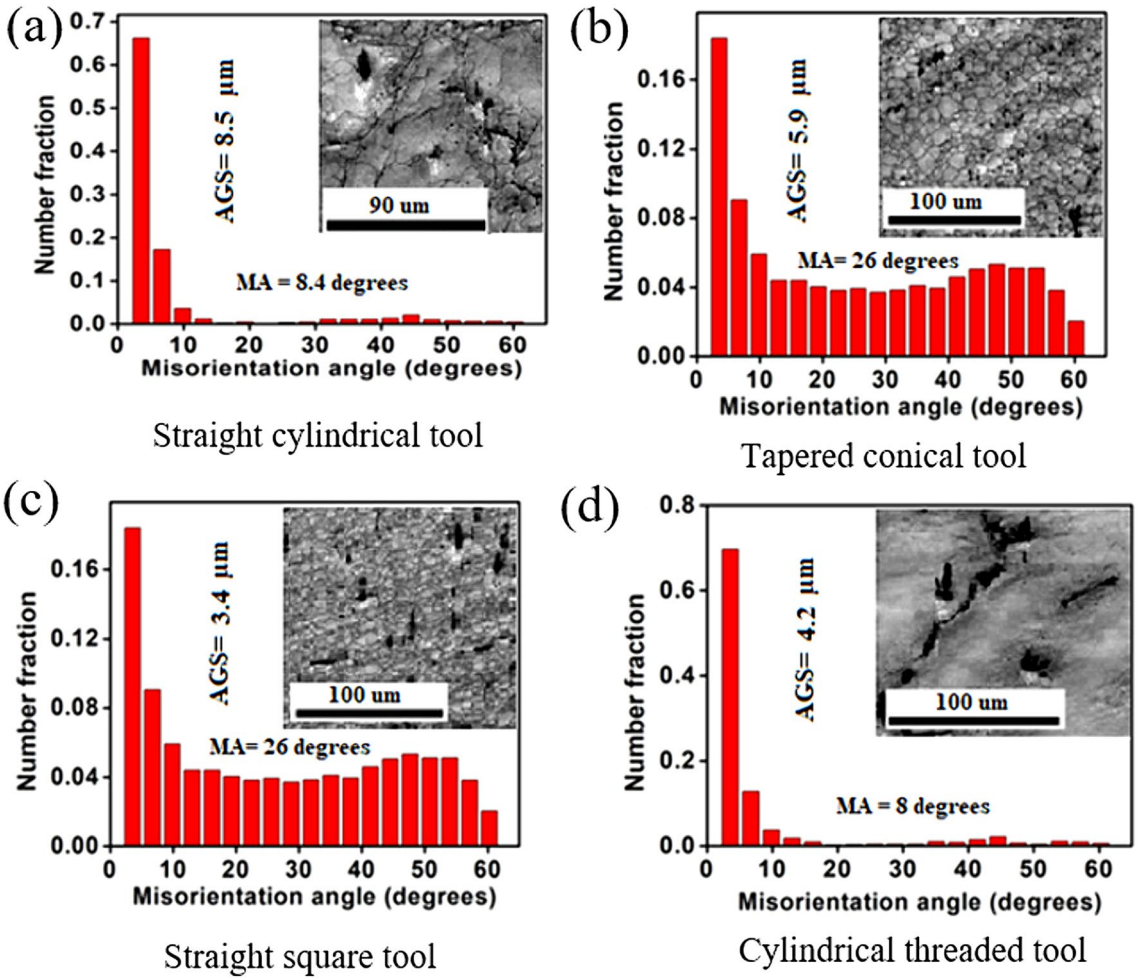

Fig. 14 Shows grain size diameter and distribution of grain boundaries for various FSW tools [88]

9 Conclusions and Scope for Future

The present review summarizes an overall view of AMCs using FSW with a few critical concerns discussed. It also addressed how to weld aluminum alloys and AMCs. The microstructure and mechanical properties of joints were studied.

FSW increased joint efficiency and good production precision are even further desirable for the non-weldable series, such as AA2000, AA6000, and AA7000. FSW is a sustainable welding technique for achieving crack-free AMCs joints. More efforts are needed to fully comprehend the impact of FSW on such materials to fulfill design and production necessities. For example, there is a need for extensive research that reflects the impact of reinforcement percentage and as well as reinforcement type on joint effectiveness. Further research is required to fully comprehend the results of FSW joints, especially for AA2124, AA2014, AA6082, and AA6092 AMCs with varying percentages of reinforcements. In addition, a thorough analysis of the shape, size, and dispersion of reinforcing particles in the nugget zone and their impact on the nugget zones strength is still lacking.

Micrographs of FSW joints disclosed the generation of new different grain sizes and the improvement of reinforcement particles in the weld zone as heat input was varied by controlling the welding parameters. Even neither general relationship has been found between the welding variables and mechanical characteristics for several types of AMCs. More research is required to define each composite welding frame for optimal mechanical properties. Also, little information is available on the strength and toughness of FSWed AMCs. More research is needed to fully understand these properties to identify the full potential of FSW joints. The influence of FSW variables on a welded joint like tensile strength and hardness has yet to be thoroughly investigated using analytical approaches.

Finally, the wear of tools has been a major concern to the proposal of the FSW process in the production industry. Researchers can try tools such as inverted taper, and square pin with threads with a proper coating material. Aircraft sectors use lighter materials that are difficult to weld without defects using conventional processes. FSW assists in welding such components without defects and with the desired strength, such as magnesium, aluminum alloys.

Acknowledgements This work was supported by the research seed Grant Ref. No. RU: EST:ME: 2022: 1 funded by REVA University Bengaluru, India. Authors acknowledge the support from REVA University for funding and providing the facilities to carry out the research.

References

1. Sachinkumar S, Narendranath S, and Chakradhar D, *AIP Conf Proc* **1943** (2018) 020118. https://doi.org/10.1063/1.5029694
2. Omid K D, Alireza A, Ghasem A R, and Mohammad J N, *J Manuf Process* **68** (2021) 616. https://doi.org/10.1016/j.jmapro.2021.05.068
3. Niraj K, and Ashish D, *Mater Today Proc* **26** (2020) 1666. https://doi.org/10.1016/j.matpr.2020.02.352
4. Sachinkumar S, Narendranath S, and Chakradhar D, *Silicon* **11** (2019) 2557. https://doi.org/10.1007/s12633-018-0044-5
5. Omar S, Hengan O, Sun W, and McCartney D G, *Mater Des* **86** (2015) 61. https://doi.org/10.1016/j.matdes.2015.07.071
6. Anton N, Fedor I, Evgenii R, Pavel P, Mikhail P, Aleksey S, Sergio T A F, and Oleg P, *J Mater Res Technol* **9** (2020) 14454. https://doi.org/10.1016/j.jmrt.2020.10.008
7. Rahul B, and Sachinkumar P, *Mater Today Proc* **82** (2023) 8. https://doi.org/10.1016/j.matpr.2022.10.129
8. Nikolai K, Volker V, and Gürel C, *J Manuf Process* **36** (2018) 571. https://doi.org/10.1016/j.jmapro.2018.10.005
9. Sachinkumar P, Narendranath S, and Chakradhar D, *Mater Today Proc* **45** (2021) 1. https://doi.org/10.1016/j.matpr.2020.09.025
10. Ilangovan M, Rajendra B, and Balasubramanian S, *Trans Nonferrous Met Soc China* **25** (2015) 1080. https://doi.org/10.1016/S1003-6326(15)63701-3
11. Uyime D, Maysa T, Carlos R O, Fernanda M Q, Aline S B, and Isold C, *Corros Sci* **131** (2018) 300. https://doi.org/10.1016/j.corsci.2017.12.001
12. Amit G, and Rameshkumar G, *Silicon* **11** (2019) 51. https://doi.org/10.1007/s12633-018-9858-4
13. Beytullah G, Erdinc K, Emel T, and Aydin S, *Mater Des* **56** (2014) 84. https://doi.org/10.1016/j.matdes.2013.10.090
14. Baidehish S, and Jinu P, *Materialia* **2** (2018) 196. https://doi.org/10.1016/j.mtla.2018.08.003
15. Texier D, Zedan Y, Amoros T, Feulvarch E, Stinville J C, and Bocher P, *Mater Des* **108** (2016) 217. https://doi.org/10.1016/j.matdes.2016.06.091
16. Mohammad R J, Hesam P, Abdollah S, Sun I H, and Matteo P, *Materials* **14** (2021) 1290. https://doi.org/10.3390/ma14051290
17. Sachinkumar P, Nagamadhu M, and Malyadri T, *Mater Today Proc* **82** (2023) 75. https://doi.org/10.1016/j.matpr.2022.11.362
18. Natrayan L, and Senthilkumar M, *Mater Today Proc* **27** (2020) 306. https://doi.org/10.1016/j.matpr.2019.11.038
19. Terry K, *An Outsider Looks at Friction Stir Welding*. Report: ANM-112N-05-06, July (2005)
20. Krishna K M, and Kumar A, *J Manuf Process* **32** (2018) 625. https://doi.org/10.1016/j.jmapro.2018.03.034
21. Khalique E A, Nagesh B M, Raju B S, and Drakshayani D N, *Mater Today Proc* **20** (2020) 108. https://doi.org/10.1016/j.matpr.2019.10.059
22. Zhe L, Wei G, Huijun L, Dongpo W, and Lei C, *J Manuf Process* **84** (2022) 1122. https://doi.org/10.1016/j.jmapro.2022.10.069
23. Meshram S D, and Reddy G M, *Def Sci J* **68** (2018) 512. https://doi.org/10.14429/dsj.68.12027
24. Long L, Chen G, Zhang S, Liu T, and Shi Q, *J Manuf Process* **30** (2017) 562. https://doi.org/10.1016/j.jmapro.2017.10.023
25. Chauhan P, Jain R, Pal S K, and Singh S B, *J Manuf Process* **34** (2018) 158. https://doi.org/10.1016/j.jmapro.2018.05.022
26. Aghajani D H, and Abdolreza S, *Sci Technol Weld Join* **23** (2018) 209. https://doi.org/10.1080/13621718.2017.1364896
27. Hamilton C, Dymek S, Kopyscianski M, Weglowska A, and Pietras A, *Metals* **8** (2018) 324. https://doi.org/10.3390/met8050324
28. Marek S W, *Arch Civ Mech Eng* **18** (2018) 114. https://doi.org/10.1016/j.acme.2017.06.002

29. Ashok B, and Murugan N, *Mater Des* **57** (2014) 383. https://doi.org/10.1016/j.matdes.2013.12.065
30. Rajana V, Durjyodhan S, Vamsikrishna K, and Barnik S R, *Mater Today Proc* **18** (2019) 5276. https://doi.org/10.1016/j.matpr.2019.07.551
31. Devaiah D, Kishore K, and Laxminarayana P, *Mater Today Proc* **5** (2018) 4607. https://doi.org/10.1016/j.matpr.2017.12.031
32. Yuvaraj K P, Ashoka V P, Haribabu L, Madhubalan R, and Boopathiraja K P, *Mater Today Proc* **45** (2021) 919. https://doi.org/10.1016/j.matpr.2020.02.942
33. Muthu K M, Maniraj J, Deepak R, and Anganan K, *Mater Today Proc* **5** (2018) 716. https://doi.org/10.1016/j.matpr.2017.11.138
34. Sachinkumar S, Narendranath S, and Chakradhar D, *Emerg Mater Res* **7** (2018) 192. https://doi.org/10.1680/jemmr.17.00047
35. Nandan R, DebRoy T, and Bhadeshia H K D H, *Prog Mater Sci* **53** (2008) 980. https://doi.org/10.1016/j.pmatsci.2008.05.001
36. Caroline S, Terra J, and Luis L S, *J Manuf Process* **68** (2021) 1395. https://doi.org/10.1016/j.jmapro.2021.06.052
37. Singh B, Saxena K, and Singhal P, *J Mater Eng Perform* **30** (2021) 8606. https://doi.org/10.1007/s11665-021-06017-3
38. Hasan M J, Mehran T E, Amir C, Reza K, and Razieh Y, *CIRP J Manuf Sci Technol* **35** (2021) 69. https://doi.org/10.1016/j.cirpj.2021.05.007
39. Yuvaraj K P, Ashoka V P, Haribabu L, Madhubalan R, and Boopathiraja K P, *Mater Today Proc* **45** (2021) 919. https://doi.org/10.1016/j.matpr.2020.02.942
40. Anna J, Jacek T, and Dariusz F, *Materials* **14** (2021) 3244. https://doi.org/10.3390/ma14123244
41. Nidhi S, Arshad N S, Zahid A K, and Mohsin T M, *Mater Manuf Process* **33** (2018) 786. https://doi.org/10.1080/10426914.2017.1388526
42. Sanjeev V, and Vinod K, *J Mech Eng Sci* **235** (2021) 1.
43. Ashu G, Madhav R, and Anirban B, *CIRP J Manuf Sci Technol* **29** (2020) 99. https://doi.org/10.1016/j.cirpj.2020.03.001
44. Zhou L, Zhang R X, Li G H, Zhou W L, Huang Y X, and Song X G, *J Manuf Process* **36** (2018) 1. https://doi.org/10.1016/j.jmapro.2018.09.017
45. Ghiasvand A, Hassanifard S, Saad S, and Varvani F A, *Sci Technol Weld Join* **26** (2021) 493. https://doi.org/10.1080/13621718.2021.1950500
46. Rajendra S, Cheraku S, Rajnish K, and Ashis K S, *Mater Today Proc* **66** (2022) 1361. https://doi.org/10.1016/j.matpr.2022.05.154
47. Kumar R, Kumar H, Kumar S, and Chohan J S, *Mater Today Proc* **48** (2022) 1594. https://doi.org/10.1016/j.matpr.2021.09.491
48. Kumar S, Chaubey S K, and Sethi D, *J Mater Eng Perform* **31** (2022) 2074. https://doi.org/10.1007/s11665-021-06315-w
49. Malleswararao N B, Varaha S V, and Hari C, *Eng Res Express* **3** (2021) 035026. https://doi.org/10.1088/2631-8695/ac1a5a
50. Jayaprakash S, Chandran S, Sathish T, Gugulothu B, Ramesh R, Sudhakar M, and Ram S, *Adv. Mater. Sci. Eng.* **2021** (2021) 1. https://doi.org/10.1155/2021/7387296
51. Dmitry O B, Mohammed A J, Wanich S, Mahmoud E A, Aleksandra S, Dariusz F, and Hamed A D, *Materials* **14** (2021) 7883. https://doi.org/10.3390/ma14247883
52. Pranesh B, Tamilselvam P, and Suresh K S, *J Mater Eng Perform* **31** (2022) 8967. https://doi.org/10.1007/s11665-022-06908-z
53. Yumeng S, Wei L, Yupeng L, Wenbiao G, and Chuan J, *Materials* **12** (2022) 408. https://doi.org/10.3390/met12030408
54. Rahul K, Kishor J, Anwar A, Murshid I, and Chiranjit S, *Mater Today Commun* **33** (2022) 104785. https://doi.org/10.1016/j.mtcomm.2022.104785
55. Nikul P, Bhatt K D, and Vishal M, *Procedia Technol* **23** (2016) 558. https://doi.org/10.1016/j.protcy.2016.03.063
56. Yang X, Liming K, Yuqing M, and Pengliang N, *Mater Charact* **174** (2021) 111022. https://doi.org/10.1016/j.matchar.2021.111022
57. Ramachandran K, Murugan N, and Shashi S, *Mater Sci Eng A* **639** (2015) 219. https://doi.org/10.1016/j.msea.2015.04.089
58. Yanying H, Huijie L, and Shuaishuai D, *Mater Sci Eng A* **804** (2021) 140587. https://doi.org/10.1016/j.msea.2020.140587
59. Ravi B, Balu N B, and Udaya P J, *Mater Today Proc* **2** (2015) 2984. https://doi.org/10.1016/j.matpr.2015.07.282
60. Chengcha D, Xue W, Qiuhong P, Kailin X, Mansheng N, and Junjian L, *J Manuf Process* **38** (2019) 122. https://doi.org/10.1016/j.jmapro.2019.01.010
61. Joao V S A, Aline F S B, Uyime D, Caruline S C M, Fernanda M Q, Maysa T, Antonello A, and Isolda C, *Corros Eng Sci Technol* **54** (2019) 575. https://doi.org/10.1080/1478422X.2019.1637077
62. Wang D, Xiao B L, Ni D R, and Ma Z Y, *Acta Metall Sinica* **27** (2014) 816. https://doi.org/10.1007/s40195-014-0143-2
63. Ahmed B, Mohammed E, and Galal N, *Int J Adv Sci Technol* **29** (2020) 1322.
64. Xiangbin W, and Diana A L, *Materialia* **24** (2022) 101508. https://doi.org/10.1016/j.mtla.2022.101508
65. Gurpreet S, Sanjeev G, Georgina M, and Neeraj S, *J Mech Sci Technol* **32** (2018) 579. https://doi.org/10.1007/s12206-018-0105-5
66. Raju P M, Ravi K, and Surjya K P, *Mater Charact* **160** (2020) 110115. https://doi.org/10.1016/j.matchar.2019.110115
67. Ahmed M M Z, Ataya S, El-Sayed S M M, Ammar H R, and Ahmed E, *J Mater Process Technol* **242** (2017) 77. https://doi.org/10.1016/j.jmatprotec.2016.11.024
68. Lin C, Chunming W, Lingda X, Xiong Z, and Gaoyang M, *Mater Des* **191** (2020) 108625. https://doi.org/10.1016/j.matdes.2020.108625
69. Taher A S, Nagi M S, Ibrahim M M, Yajun Y, Xiaoyuan J, Xu S, and Jianxin Z, *Vacuum* **188** (2021) 110216. https://doi.org/10.1016/j.vacuum.2021.110216
70. Salehi M, Saadatmand M, and Aghazadeh M J, *Trans Nonferrous Met Soc China* **22** (2012) 1055. https://doi.org/10.1016/S1003-6326(11)61283-1
71. Beygi R, Pouraliakbar H, Torabi K, Eisaabadi B G, Fallah V, Kim S K, Shi R, and Silva L F M, *J Manuf Process* **70** (2021) 152. https://doi.org/10.1016/j.jmapro.2021.08.049
72. Taher A S, Jianxin Z, Xu S, Yajun Y, and Xiaoyuan J, *Proc Manuf* **37** (2019) 555. https://doi.org/10.1016/j.promfg.2019.12.088
73. Sachinkumar S, Narendranath S, and Chakradhar D, *Mater Today Proc* **20** (2020) A1. https://doi.org/10.1016/j.matpr.2020.01.266
74. Yahya B, Huseyin U, and Serdar S, *J Compos Mater* **45** (2011) 2237. https://doi.org/10.1177/0021998311401067
75. Huijie L, Yanying H, Chao D, and Dusan P S, *Mater Character* **123** (2017) 9. https://doi.org/10.1016/j.matchar.2016.11.011
76. Behrooz R, Kamran D, and Seyyed E M, *J Manuf Process* **52** (2020) 152. https://doi.org/10.1016/j.jmapro.2020.01.046
77. Zhenglin D, Hui C, Ming J T, Guijun B, and Chee K C, *J Manuf Process* **36** (2018) 33. https://doi.org/10.1016/j.jmapro.2018.09.024
78. Durjyodhan S, Uttam A, Tanmoy M, Shashank S, and Barnik S R, *Mater Today Proc* **46** (2021) 9180. https://doi.org/10.1016/j.matpr.2020.01.198
79. Kalaiselvan K, Dinaharan I, and Murugan N, *Mater Des* **55** (2014) 176. https://doi.org/10.1016/j.matdes.2013.09.067
80. Logendran D, Chandramohan D, and Sathish T, *Mater Today Proc* **33** (2020) 4663. https://doi.org/10.1016/j.matpr.2020.08.310
81. Subramanya R P B, Arun S, Mervin H, and Shrikantha R, *Mater Today Proc* **24** (2020) 1183. https://doi.org/10.1016/j.matpr.2020.04.432

82. Mohammad S M I, Kaveh M, Mohammad A A, Sufian R, Mohd R M, Farazila Y, Mohd J, Nukman Y, and Mohd S A K, *J Mater Res Technol* **15** (2021) 2735. https://doi.org/10.1016/j.jmrt.2021.09.037
83. Marie N, Avettand F, and Aude S, *Mater Charact* **120** (2016) 1. https://doi.org/10.1016/j.matchar.2016.07.010
84. Liua H J, Feng J C, Fujii H, and Nogi K, *Int J Mach Tools Manuf* **45** (2005) 1635. https://doi.org/10.1016/j.ijmachtools.2004.11.026
85. Devender K, Denny J O, Uttam A, Tanmoy M, Barnik S R, and Subhash C S, *Mater Today Proc* **46** (2021) 9378. https://doi.org/10.1016/j.matpr.2020.02.933
86. Makeshkumar M, Surender S R, Arunprakash S, Madesh R, Sasi M, and Sudharsan K, *Mater Today Proc* **47** (2021) 5239. https://doi.org/10.1016/j.matpr.2021.05.563
87. Huaqiang L, Yulong W, and Shengdan L, *Mater Charact* **146** (2018) 159. https://doi.org/10.1016/j.matchar.2018.09.043
88. Sachinkumar S, Narendranath S, and Chakradhar D, *Trans Indian Inst Met* **73** (2020) 2269. https://doi.org/10.1007/s12666-020-02035-2
89. Contorno D, Faga M G, Fratini L, Settineri L, and Gautier C G, *Key Eng Mater* **410** (2009) 235. https://doi.org/10.4028/www.scientific.net/KEM.410-411.235
90. Umesh Kumar S, and Avanish Kumar D, *Mater Today Proc* **47** (2021) 2720. https://doi.org/10.1016/j.matpr.2021.02.811
91. Wang D, Xiao B L, Wang Q Z, and Ma Z Y, *J Mater Sci Technol* **30** (2014) 54. https://doi.org/10.1016/j.jmst.2013.09.018
92. Lan Z, Huilong Z, Shengci L, Hongjin Z, Jiqiang C, and Liang Q, *Int J Fatigue* **135** (2020) 105556. https://doi.org/10.1016/j.ijfatigue.2020.105556
93. Won B L, Yun M Y, and Seung B J, *Mater Trans* **45** (2004) 170. https://doi.org/10.2320/matertrans.45.1700
94. Liu H J, Feng J C, Fujii H, and Nogi K, *Int J Mach Tools Manuf* **45** (2005) 1635. https://doi.org/10.1016/j.ijmachtools.2004.11.026
95. Hu Z L, Wang X S, Pang Q, Huang F, Qin X P, and Hua L, *Mater Charact* **99** (2015) 180. https://doi.org/10.1016/j.matchar.2014.11.015
96. Subramanya R P, Arun S, Mervin A H, and Shrikantha S R, *Weld World* **66** (2022) 93. https://doi.org/10.1007/s40194-021-01187-z
97. Amit G, and Ramesh G, *Metallogr Microstruct Anal* **7** (2018) 524. https://doi.org/10.1007/s13632-018-0468-8
98. Srinivasa Rao M S, Ravi Kumar B V R, and Manzoor H M, *Mater Today Proc* **4** (2017) 1394. https://doi.org/10.1016/j.matpr.2017.01.161
99. Krasnowski K, Hamilton C, and Dymek S, *Arch Civ Mech Eng* **15** (2015) 131. https://doi.org/10.1016/j.acme.2014.02.001
100. Kumar A, Mahapatra M M, Jha P K, Mandal N R, and Devuri V, *Mater Des* **59** (2014) 406. https://doi.org/10.1016/j.matdes.2014.02.063
101. Marzoli L M, Strombeck A V, Santos J F, Gambaro C, and Volpone L M, *Compos Sci Technol* **66** (2006) 363. https://doi.org/10.1016/j.compscitech.2005.04.048
102. Cavaliere P, Cerri E, Marzulli L, and Santos J, *Appl Compos Mater* **11** (2004) 247. https://doi.org/10.1023/B:ACMA.0000035478.71092.ec
103. Ceschini L, Boromei I, Minak G, Morri A, Tarterini F, and Composites Part A, *Appl Sci Manuf* **38** (2007) 1200. https://doi.org/10.1016/j.compositesa.2006.06.009
104. Minak G, Ceschini L, Boromei I, and Ponte M, *Int J Fatigue* **32** (2010) 218. https://doi.org/10.1016/j.ijfatigue.2009.02.018
105. Periyasamy P, Mohan B, and Balasubramanian V, *J Mater Eng Perform* **21** (2012) 2417. https://doi.org/10.1007/s11665-012-0176-5
106. Periyasamy P, Mohan B, Balasubramanian V, Rajakumar S, and Venugopal S, *Trans Nonferrous Met Soc China* **23** (2013) 942. https://doi.org/10.1016/S1003-6326(13)62551-0
107. Dinaharan I, and Murugan N, *Met Mater Int* **18** (2012) 135. https://doi.org/10.1007/s12540-012-0016-z
108. Feng A H, Xiao B L, and Ma Z Y, *Compos Sci Technol* **68** (2008) 2141. https://doi.org/10.1016/j.compscitech.2008.03.010
109. Rohan A, Piyush G, Dinesh S, and Hitesh D, *Mater. Today Proc* **18** (2020) 4092. https://doi.org/10.1016/j.matpr.2019.07.353
110. Ni D R, Chen D L, Wang D, Xia B L, and Ma Z Y, *Mater Sci Eng A* **608** (2014) 1. https://doi.org/10.1016/j.msea.2014.04.060
111. Akeem Y A, Fadi A B, and Zuhair M G, *J Manuf Process* **33** (2018) 111. https://doi.org/10.1016/j.jmapro.2018.04.019
112. Qiushi G, Hua Y, Yang Q, Peilei Z, Jialong G, Zhengfei C, and Zhishui Y, *Opt Laser Technol* **113** (2019) 182. https://doi.org/10.1016/j.optlastec.2018.12.046
113. Adel M H, Mohammed A, Tarek Q, and Ahmed G, *Mater Manuf Process* **27** (2012) 1419. https://doi.org/10.1080/10426914.2012.700156
114. Bahuguna S, Arya P K, and Patel V K, *J Mech Eng* **70** (2020) 21. https://doi.org/10.2478/scjme-2020-0017
115. Biing H Y, Hsien C T, Fuang Y H, and Long C L, *Int J Mach Tools Manuf* **45** (2005) 251. https://doi.org/10.1016/j.ijmachtools.2004.08.015
116. Seyed S M, Mohammad A, Soheil E, Kord S, Hamouda A M S, Praveennath G K, and Keshavamurthy R, *J Alloys Compd* **712** (2017) 795. https://doi.org/10.1016/j.jallcom.2017.04.114
117. Mohammad H S, Mostafa A, Parviz A, and Abolfazl K, *Int J Adv Manuf Technol* **91** (2017) 1391. https://doi.org/10.1007/s00170-016-9853-0
118. Shindo D J, Rivera A R, and Murr L E, *J Mater Sci* **37** (2002) 4999. https://doi.org/10.1023/A:1021023329430
119. Tracie P, *Acta Astronaut* **93** (2014) 366. https://doi.org/10.1016/j.actaastro.2013.07.023
120. Xiao L, Xiu L, Peng Y, Shi Q, Yong Z, Ming W, Yao C, and Dong X, *Opt Laser Technol* **78** (2016) 87. https://doi.org/10.1016/j.optlastec.2015.10.005
121. Sachinkumar S, Narendranath S, and Chakradhar D, *Trans Indian Inst Met* **74** (2021) 1303. https://doi.org/10.1007/s12666-021-02214-9
122. Shaik M, Jimmy K, Raviraj V, and Jha P K, *J Alloys Compd* **826** (2020) 154184. https://doi.org/10.1016/j.jallcom.2020.154184
123. Akbar H, *Arch Civ Mech Eng* **19** (2019) 137. https://doi.org/10.1016/j.acme.2018.09.009
124. Qi W, Mingyang L, Yuanhang G, Jianfu S, Hanlu W, and Yongqin C, *Nucl Mater Energy* **25** (2020) 100804. https://doi.org/10.1016/j.nme.2020.100804
125. Guoa J, Amira S, Gougeon P, and Chen X G, *Mater Charact* **62** (2011) 865. https://doi.org/10.1016/j.matchar.2011.06.007
126. Zhikang S, Xinqi Y, Zhaohua Z, Lei C, and Yuhuan Y, *Mater Des* **49** (2013) 181. https://doi.org/10.1016/j.matdes.2013.01.066